Chemical Geology 479 (2018) 102–112

Contents lists available at ScienceDirect

Chemical Geology

journal homepage: www.elsevier.com/locate/chemgeo

Sr–Nd isotopic geochemistry of Holocene sediments from the South Yellow Sea: Implications for provenance and monsoon variability

Bangqi Hu[a,b,c,*], Jun Li[a,b], Jingtao Zhao[a], Hong Yan[c], Liang Zou[a], Fenglong Bai[a], Fangjian Xu[d], Xuebo Yin[e], Gangjian Wei[f]

[a] Key Laboratory of Marine Hydrocarbon Resources and Environmental Geology, Ministry of Land and Resources, Qingdao Institute of Marine Geology, China Geological Survey, Qingdao 266071, China
[b] Laboratory for Marine Mineral Resources, Qingdao National Laboratory for Marine Science and Technology, Qingdao 266071, China
[c] State Key Laboratory of Loess and Quaternary Geology, Institute of Earth Environment, Chinese Academy of Sciences, Xi'an 710075, China
[d] School of Geosciences, China University of Petroleum, Qingdao 266580, China
[e] Key Laboratory of Marine Geology and Environment, Institute of Oceanology, Chinese Academy of Sciences, Qingdao 266071, China
[f] State Key Laboratory of Isotope Geochemistry, Guangzhou Institute of Geochemistry, Chinese Academy of Sciences, Guangzhou 510640, China

ARTICLE INFO

Keywords:
Sr–Nd isotopes
Provenance
Monsoon
Yellow Sea
Holocene

ABSTRACT

Elemental geochemical and Sr–Nd isotopic signatures are used to decipher terrigenous sediments provenances and transport mechanisms in the South Yellow Sea during the Holocene. $^{87}Sr/^{86}Sr$ ratios in the Chinese and Korean riverine sediments overlap each other, whereas εNd values of Korean riverine sediments are generally less radiogenic in comparison to the Changjiang and Huanghe. Moreover, εNd values of these two large rivers appear unaffected by mineral sorting and are relative stable during the Holocene. We propose a three end-members (i.e., the Changjiang, the Huanghe, and Korean rivers) mixing model to explain sediment provenances in the Central Yellow Sea Mud (CYSM). Mixing calculations show that the Huanghe is the major sediment contributor to the CYSM before ~8 ka (thousand years before 1950 CE), whereas the Changjiang has become the predominant sediment source after ~8 ka. Holocene changes in riverine sediment supplies to the CYSM are closely related to the oceanic circulation, monsoon climate, and drainage changes. After examining several hypotheses to explain the variations in $^{87}Sr/^{86}Sr$ ratios of Core YSC-1 during the past ~8 kyr, we tentatively attribute that to changes in the erosion patterns of the Changjiang Basin. This in turn is associated with the asynchronous evolution of monsoon precipitation in the upper (Indian Summer Monsoon) and middle-lower Changjiang (East Asian Summer Monsoon). Therefore, our results highlight significant influences of monsoon climate on erosion patterns within the Changjiang catchment at millennial timescales.

1. Introduction

Large rivers of East Asian, originating in the Himalaya and the Tibetan Plateau, discharge an estimated 20% of the global river sediment flux (Milliman and Farnsworth, 2011). Tectonics (active uplift) and climate (monsoon-related intense precipitation) are two main agents governing the high sediment yields within these large river basins on geological time scales (Clift et al., 2008; Clift, 2010). However, the relative roles of tectonic and climatic factors on erosion and weathering remain uncertain, resulting from the complex interplays and threshold effects in this coupled system (West et al., 2005; Willenbring and von Blanckenburg, 2010; Cogez et al., 2015). Continental shelves are the key interfaces between terrestrial sediment source areas and deep-sea depositional systems, by which they can serve as capacitors or conveyors in the sediment-rounting systems, depending on the shelf width, climatic forcings, and timescales (Covault et al., 2011; Covault and Fildani, 2014). Commonly, continental shelves on passive margin have long transfer zones containing sediment sinks that can store sediment temporarily or permanently, and thus sedimentary deposited on them can serve as natural "recorders" of environmental signals at intermediate timescale (centennial to millions of years) (Romans et al., 2016). However, complex processes occur in the erosion, transport and storage of sediments (as well as their interactions) from the upland to the marginal seas, which probably disturb the original environmental signals and cause troubles for paleoclimatic reconstruction based on the sedimentary record.

* Corresponding author at: Key Laboratory of Marine Hydrocarbon Resources and Environmental Geology, Ministry of Land and Resources, Qingdao Institute of Marine Geology, China Geological Survey, Qingdao 266071, China.
E-mail address: bangqihu@gmail.com (B. Hu).

https://doi.org/10.1016/j.chemgeo.2017.12.033
Received 8 April 2017; Received in revised form 29 November 2017; Accepted 31 December 2017
Available online 05 January 2018

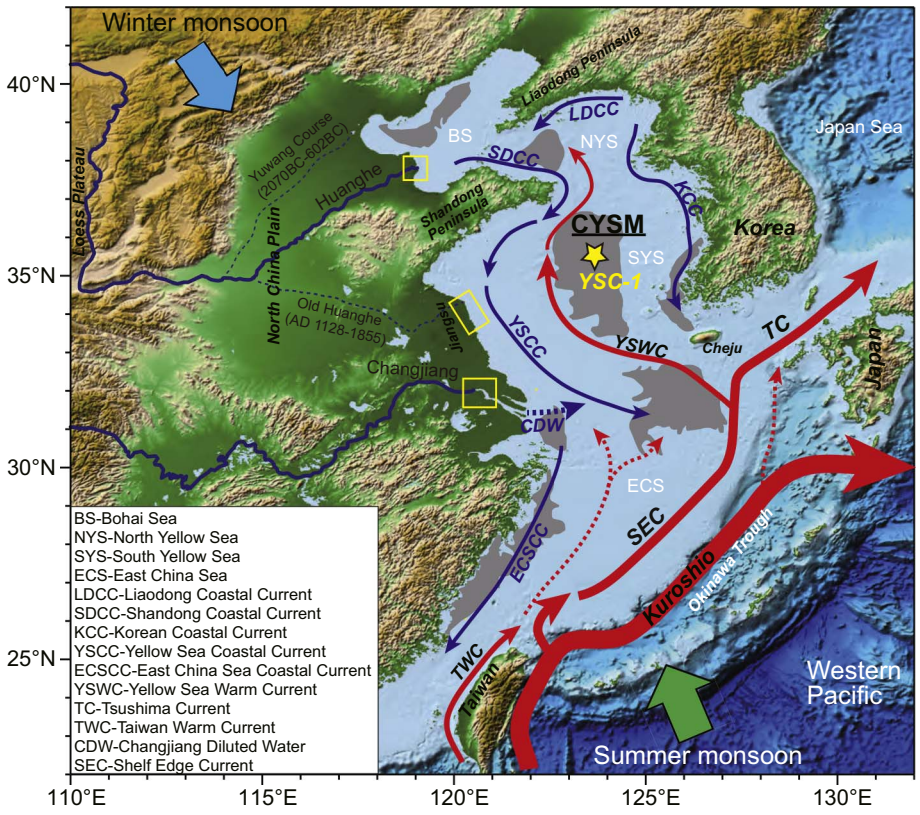

Fig. 1. Schematic illustration of the topography and winter oceanic currents (modified from Li et al., 2016) in the East China Seas. The red lines indicate the warm current systems, whereas the blue lines indicate the cold coastal currents. Dashed red lines are the branches from the main warm current. Shaded areas are the muddy depositional areas and CYSM is the Central Yellow Sea Mud. Riverine samples from the Changjiang, the Huanghe and the Old Huanghe (yellow rectangle) and Core YSC-1 (yellow star) are also shown. (For interpretation of the references to colour in this figure legend, the reader is referred to the web version of this article.)

The Yellow Sea is a semi-enclosed shallow epicontinental shelf surrounded by mainland China and Korean Peninsula. Annually, the Yellow Sea received a huge amount of fluvial sediments mainly from two global large rivers [i.e. the Huanghe (Yellow River) and Changjiang (Yangtze River)], as well as some small rivers in Korea Peninsula. Although the Changjiang and Huanghe do not enter the Yellow Sea directly at present, they have been considered as the predominant sediment sources of Yellow Sea (Lee and Chough, 1989; Yang et al., 2003; Hu et al., 2011; Qiao et al., 2017). Under the combined effects of tide, wave/storm and current, several muddy depositional areas are developed in the broad and shallow shelf of Yellow Sea during the Holocene sea-level highstand (Lee and Chough, 1989; Li et al., 2014a). The Central Yellow Sea Mud (CYSM) is one of the largest muddy depositional areas on the Yellow Sea shelf (Fig. 1), resulting from the large accommodation space and abundant sediment supplies. Mud deposits in the CYSM are not only the outstanding archives of Holocene climatic and environmental changes in the adjacent continent, but also preserve essential information on the past ocean circulation patterns (Kim and Kucera, 2000; Xiang et al., 2008; Hu et al., 2012b; Ge et al., 2014; Li et al., 2014b; Wang et al., 2014; Lim et al., 2015b). Therefore, the CYSM has attracted much attention with respect to its formation mechanism and evolution history since the 1990s.

By identifying and characterizing the terrigenous sediment source areas of CYSM, detailed information can be obtained on the provenance and transport mechanisms, which are fundamental, but yet remain considerable debate (Yang et al., 2003). Considering low sediment load of Korean rivers, it has been originally presumed the CYSM is mainly supplied by the Chinese rivers (i.e., the Huanghe and Changjiang) (e.g., Lee and Chough, 1989; Alexander et al., 1991; Park and Khim, 1992). Subsequently, much efforts have been expended to discriminate surface sediment provenance in the coastal and shelf mud depositions of Yellow Sea, including geochemical (Lim et al., 2006; Yang and Youn, 2007; Lim et al., 2014; Jung et al., 2016), mineralogical (Wei et al., 2003; Li et al., 2014c), and magnetic (Wang et al., 2010; Wang et al., 2017) techniques. Almost all of them suggested that the CYSM might be a "multi-sourced deposits" consists of a mixture of Chinese large rivers and Korean small rivers, however, the relative contributions from different sources remain unclear. Several studies have attempted to decipher the changes in detrital sediment supply to the CYSM during the Holocene but rarely have any consensus been achieved, partly resulting from proxies' susceptibility, analytical error (e.g., clay minerals), and/or insufficient dating points (Yang and Youn, 2007; Lan et al., 2009; Li et al., 2014b; Wang et al., 2014; Lim et al., 2015b).

Strontium (Sr)–neodymium (Nd) isotopic ratios ($^{87}Sr/^{86}Sr$ and εNd) are widely used to decipher the source areas of terrigenous sediments, because the $^{87}Sr/^{86}Sr$ and εNd of continental detritus mainly depend on their Rb/Sr and Sm/Nd ratios and the rock ages (Frank, 2002; Grousset and Biscaye, 2005). Sr isotope composition, besides the source heterogeneity, is also associated with changes in chemical weathering intensity and hydrodynamic sorting effect (Colin et al., 2006; Cole et al., 2009; Révillon et al., 2011; Ali et al., 2015). In contrast, Nd is relatively immobile element during surficial processes, and it is often assumed that there is no significant dependence of εNd on grain size or chemical weathering (Tütken et al., 2002; Meyer et al., 2011; Garçon et al., 2014; Bayon et al., 2015; Lim et al., 2015a; Rao et al., 2017). Although Sr–Nd isotopic compositions of detrital fractions have been proven to be useful tracers on sediment provenance in the East China Seas (Dou et al., 2012; Hu et al., 2012a; Li et al., 2015; Dou et al., 2016; Bi et al., 2017; Rao et al., 2017), comprehensive provenance discrimination based on Sr–Nd isotopic compositions has not been conducted for core sediments in the CYSM until now. In this study, we use elemental and Sr–Nd isotopic compositions from Core YSC-1 (1) to constrain the provenance of terrigenous material in the CYSM and their transport mechanisms during the Holocene and (2) to discuss the potential monsoon-climate influences on the erosion pattern within the Changjiang basin at millennial timescales.

2. Regional settings

The Yellow Sea is a shallow, semi-closed, epicontinental sea

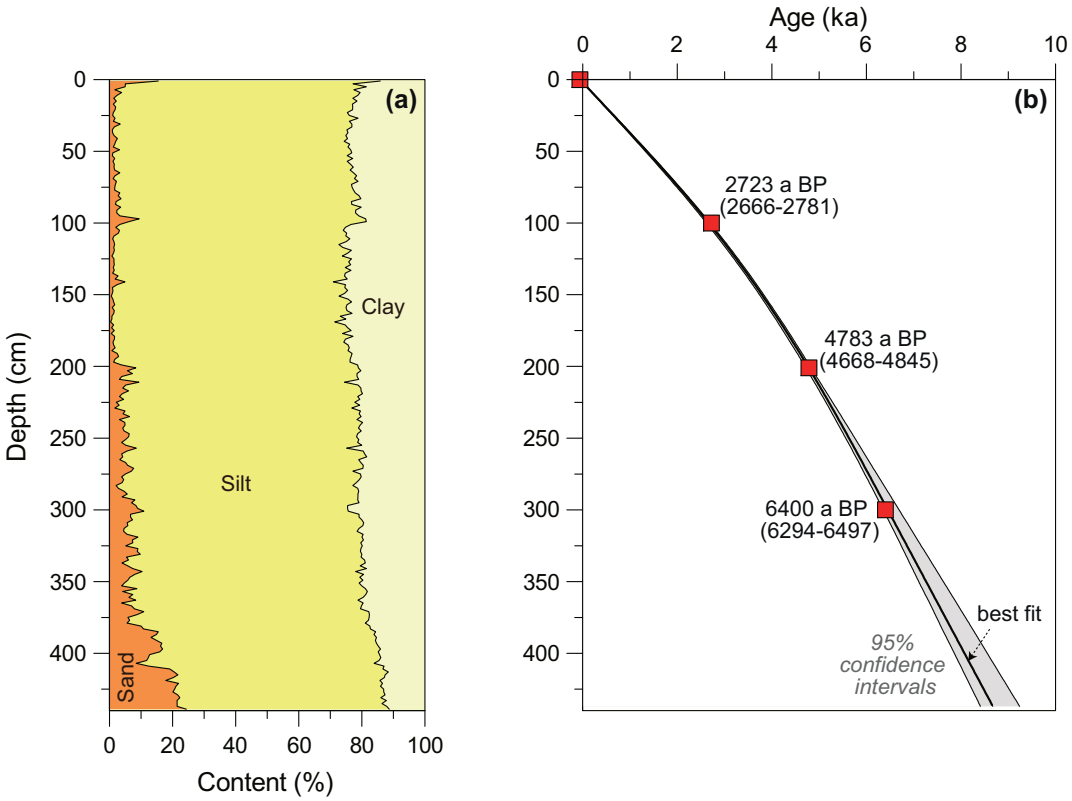

Fig. 2. (a) Vertical lithology profile and (b) age model of Core YSC-1 in the South Yellow Sea. Red squares are samples selected for AMS ^{14}C dating, we assign the calibrated 14C age of −60 ± 5 a BP at 0 cm depth. Gray shaded areas of the age-depth curve correspond to the 95% confidence intervals as output by the CLAM 2.2 software (Blaauw, 2010). (For interpretation of the references to colour in this figure legend, the reader is referred to the web version of this article.)

between the Korean peninsula and China, with an average water depth of 55 m and a maximum depth of 100 m. It is separated from the Bohai Sea to the west by the Bohai Strait, and from the East China Sea to the south by a line connecting the north edge of the Changjiang mouth with the Cheju Island. The Shandong Peninsula separates the South Yellow Sea (SYS) from the North Yellow Sea (NYS). The seafloor of Yellow Sea was subaerially exposed during the Last Glacial Maximum (LGM), when the paleo-coastal zone moved between 135 and 150 m isobaths (Li et al., 2014a). Recent studies have shown that sea-level reached to about −15 m after a rapid sea-level during 9–8 ka in the East China Seas region, then followed by decelerated sea-level rising until ~7 ka (Smith et al., 2011; Wang et al., 2013). As the postglacial sea-level rising, several mud depositional areas, including the CYSM, the Shandong Peninsula mud wedge (SMW), the southeastern Yellow Sea Mud (SEYSM), and the East China Sea Distal Mud (ECSDM), have developed under a complex sedimentary environment influenced by currents, tides, and storm waves (Li et al., 2014a).

Both of water properties and general circulation in the Yellow Sea display significant seasonal variability, resulting from the shallow water depth and monsoon climate conditions (Li et al., 2016). The East Asian monsoon is robust and northeasterly in winter, while mild and southwesterly in summer. In winter, the vertical distributions of temperature and salinity in the Yellow Sea are quite uniform due to the strong vertical mixing induced by the East Asian winter monsoon. The general circulation pattern of Yellow Sea in winter is characterized by the northwestward Yellow Sea Warm Current (YSWC) along the western side of Yellow Sea Trough (50–70 m water depth), and the southward Yellow Sea Coastal Current (YSCC) and Korean Coastal Current (KCC) along the Chinese and Korean coasts (Fig. 1). In summer, the Yellow Sea Cold Water Mass (YSCWM), strong thermocline, and strong temperature fronts are the most important physical features. The YSWC almost disappears in summer, partially related to the presence of the YSCWM in the central Yellow Sea. In addition, the Changjiang Diluted Water (CDW) spreads eastwards over the broad area of the East China Seas, reaching as far as the Cheju Island and Tsushima Strait (Moon et al., 2009).

The drainage systems that feed the Yellow Sea are mainly the Huanghe and Changjiang in China and small rivers in the Korean Peninsula. The Huanghe watershed is located on the North China carton, where most of the outcropping rocks formed during the Precambrian to Quaternary (Hu et al., 2012a). About 44% of the Huanghe watershed is covered by the Loess Plateau, with an area of ~ 440,000 km^2. The Changjiang drainage basin contains Paleozoic carbonate rocks, felsic metamorphic rocks, and Quaternary clastic rocks (Yang et al., 2007a). Small river basins in Korea Peninsula consist predominantly of Jurassic–Cretaceous granites and Precambrian gneisses, with minor proportions of limestone, schist, volcanic rocks, and phyllites (Lim et al., 2015a). In addition, the Huanghe directly emptied into the Yellow Sea during the period of AD1128–1855, and formed a huge delta (the Old Huanghe Delta) on the Jiangsu coast. After the Huanghe changed its lower course to the Bohai Sea in 1855 CE, the Old Huanghe Delta has suffered from intensive erosion and supplied huge amounts of sediment to the adjacent seas (Hu et al., 2014).

3. Material and methods

3.1. Sampling and age model

Core YSC-1 (123°40′E, 35°32′N; core length, 437 cm; water depth, 76.2 m) was recovered from the central Yellow Sea by D/V KAN407 in September 2010 (Fig. 1). For the comparison, thirteen riverine bedload sediments were collected from the low reaches of Huanghe (5 samples) and Changjiang (3 samples), as well as the estuary of the Old Huanghe

Table 1
Isotopic and geochemical data of Core YSC-1 from the South Yellow Sea.

Samples	Depth (cm)	Age (ka) (± 2σ)	Mz (Φ)	$^{87}Sr/^{86}Sr$ (± 2σ × 10^6)	$^{143}Nd/^{144}Nd$ (± 2σ × 10^6)	εNd	CIA	Rb/Sr	$\delta^{13}C$ (‰)	BIT[a]
YCS1-3	5	0.1 ± 0.01	6.67	0.719291 (10)	0.511991 (4)	− 12.6	60.94	1.19	− 21.5	0.22
YCS1-23	45	1.2 ± 0.02	7.05	0.718692 (8)	0.512016 (4)	− 12.1	59.56	1.24	− 21.8	0.19
YCS1-43	85	2.3 ± 0.04	6.95	0.719140(8)	0.512002(5)	− 12.4	59.73	1.22	− 22.0	0.18
YCS1-63	125	3.2 ± 0.04	7.01	0.718207 (8)	0.512004 (4)	− 12.4	58.35	1.12	− 22.0	0.16
YCS1-83	165	4.1 ± 0.05	7.21	0.717877 (7)	0.511992 (6)	− 12.6	58.83	1.12	− 22.3	0.17
YCS1-103	205	4.9 ± 0.06	6.97	0.717505 (8)	0.511999 (5)	− 12.5	57.40	1.00	− 21.7	0.19
YCS1-123	245	5.5 ± 0.09	6.74	0.717462 (6)	0.511977 (5)	− 12.9	58.28	1.05	− 21.8	0.18
YCS1-143	285	6.2 ± 0.14	6.86	0.718325 (8)	0.511977 (5)	− 12.9	60.00	1.15	− 22.0	0.19
YCS1-163	325	6.9 ± 0.21	6.65	0.718084 (8)	0.511971 (5)	− 13.0	60.11	1.11	− 21.2	0.18
YCS1-173	345	7.2 ± 0.25	6.54	0.718738 (9)	0.511976 (4)	− 12.9	61.04	1.18	− 21.9	0.16
YCS1-183	365	7.5 ± 0.29	6.71	0.718348 (10)	0.511981 (4)	− 12.8	60.24	1.08	− 22.2	0.18
YCS1-191	381	7.8 ± 0.32	6.33	0.719268 (9)	0.511979 (7)	− 12.9	62.42	1.22	− 22.8	0.14
YCS1-199	397	8.0 ± 0.34	5.91	0.719017 (9)	0.511936 (4)	− 13.7	60.96	0.99	− 22.5	0.23
YCS1-207	413	8.3 ± 0.37	5.61	0.718054 (5)	0.511926 (4)	− 13.9	55.78	0.69	− 23.1	0.21
YCS1-215	429	8.5 ± 0.40	5.63	0.718125 (7)	0.511959 (4)	− 13.2	55.49	0.70	− 23.7	0.27
YCS1-219	437	8.7 ± 0.41	5.60	0.718366 (9)	0.511961 (4)	− 13.2	55.29	0.67	− 23.7	0.30

[a] BIT is the branched vs. isoprenoid tetraether index (Ge et al., 2014).

(5 samples) (Fig. 1). These samples were obtained from surface muddy channels or bed deposits by a grabber to avoid contamination from bank sediments. The upper part of Core YSC-1 is composed of gray to dark gray clayey silt, whereas the lower part is mainly silty sand (Fig. 2a). Mixed benthic foraminifera from three horizons were picked for accelerator mass spectrometry (AMS) ^{14}C dating at Beta Analyses Company, USA. The grain size, clay minerals, and AMS ^{14}C data were reported in Li et al. (2014b). Here, we recalibrated all radiocarbon dates to calendar years before present (1950 CE) using the online program Calib 7.10, with an updated calibration curve Marine13.14c (Reimer et al., 2013) and a global marine reservoir effect (400 a) (Fig. 2b). Since Core YSC-1 was collected in 2010 CE, we assign the calibrated ^{14}C age of − 60 ± 5 a BP at 0 cm depth. Using these three AMS ^{14}C dates and − 60 ± 5 a BP for 0 cm depth, we constructed a new age-depth model by fitting a smooth spline curve (with a default smoothing factor of 0.3) with the CLAM 2.2 software (Blaauw, 2010) (Fig. 2b). The CLAM age model gives the "best" age and 95% confidence intervals generated by 1000 Monte Carlo simulations of the multi-modal ^{14}C calibration age distributions using a non-normalized, two standard deviation calibration range as opposed to a simple, Gaussian distribution (Blaauw, 2010). This method provides a smoother outline of age model and is considered to produce a more realistic model of the sedimentation process compared to the linear interpolation method. The age model for Core YSC-1 spans the period from 8673 ± 410 a BP to present, all ages before ca. 6.5 ka are extrapolated beneath the lowest ^{14}C sample, and thus uncertainty increases from ± 200 a at an age of ~6.8 ka BP to ± 410 a at the base of the core (Fig. 2b). Vertical lithology of Core YSC-1 exhibits a similar fining-upward succession with the adjacent cores (e.g., CC02, YE-2, ZY-1, ZY-2, ZY-3, EZ06-1) (Kim and Kucera, 2000; Xiang et al., 2008; Hu et al., 2012b; Lim et al., 2015b), and the age-model of YSC-1 is comparable with these cores. Considering the uncertainty of the age model, we aim to discuss the long-term trend of provenance shifts and its implications for environmental changes at millennial timescale.

3.2. Elemental analysis

A total of 110 samples of Core YSC-1 was selected for geochemistry measurements. The bulk samples were oven dried at 50 °C for 24 h and then powdered to < 200 meshes with an agate mortar and pestle. After oxidation of the organic matter with 5% H_2O_2 for 12 h at room temperature, about 200 mg bulk samples were leached with 0.25 N HCl (hydrochloric acid) for 24 h at 50 °C to eliminate the effect of carbonate and ferromanganese. The detrital residues were rinsed three times with ultrapure water and centrifuged, and the supernatant was removed. The resulted detrital fractions were digested using an HNO_3 + HF mixture, and finally dissolved in a 2 N HCl solution. Major elements were measured on an inductively coupled plasma optical emission spectrometers (ICP-OES, IRIS Intrepid II) at Key Laboratory of Marine Geology and Environment, Institute of Oceanology, Chinese Academy of Sciences. Trace elements were measured on an inductively coupled plasma mass spectrometer (ICP-MS, Elan DRC II) at the same laboratory. Discrepancies between the determined and certified values of the national geostandards GBW07315 and GBW07316 were < 5%.

The Chemical Index of Alteration (CIA) is used to quantify the chemical weathering degree experienced by sediments, referring to the progressive loss of mobile elements such as Na, Ca, and K (Nesbitt and Young, 1982). Using molecular proportions, the CIA is calculated as follows:

$$CIA = 100 \times \left(\frac{Al_2O_3}{Al_2O_3 + CaO* + Na_2O + K_2O} \right) \quad (1)$$

where CaO* represents CaO associated with the silicate fraction only and is corrected for carbonate and phosphate (apatite) according to McLennan (1993). Rb/Sr ratios of sediment can also be used to reflect the weathering intensity and/or mineral sorting, because Sr behaves like Ca and is liberated to the fluid, while Rb is analogous to K and tends to stay with the residue (Cole et al., 2009).

3.3. Sr–Nd isotopic analysis

Twenty-nine pretreated Core YSC-1 and riverine samples were selected for further Sr–Nd isotopic analysis (Table 1 and Table 2). Sr–Nd isotopic measurements were performed on a Micro-Mass Isoprobe multi-collector–inductively coupled plasma–mass spectrometer (MC–ICP–MS) at the State Key Laboratory of Isotope Geochemistry, Guangzhou Institute of Geochemistry, Chinese Academy of Sciences. For the Sr–Nd isotopic analysis, the sample solution was then loaded into a column filled with AG50-X8 cation resin. Both Sr and REEs were trapped on the column. The column was rinsed with 2 N of HCl eluent. Sr and REEs were de-trapped from the column using 2 N and 3 N HCl, respectively. The de-trapped REEs were further concentrated using an RE Spec column, and subsequently an LN Spec (HDEHP-based) column was used to separate Nd from REEs. $^{88}Sr/^{86}Sr$ = 0.1194 was adopted to calibrate mass bias during the Sr isotope measurements, and the NBS SRM 987 standard was repeatedly measured with the samples to monitor the quality of the measurements, yielding an average $^{87}Sr/^{86}Sr$ of 0.710220 ± 9 (2σ) (N = 12). Mass bias during Nd isotope measurements was normalized using $^{146}Nd/^{144}Nd$ = 0.7219. A standard Nd solution, JNdi-1, was repeatedly measured together with the samples,

Table 2
Sr–Nd isotopes of the Huanghe, Changjiang, and Old Huanghe sediments.

Rivers	Samples	$^{87}Sr/^{86}Sr$ (± 2σ × 10^6)	$^{143}Nd/^{144}Nd$ (± 2σ × 10^6)	εNd	References
Huanghe Bedload	HH-1	0.715201 (7)	0.512019 (9)	− 12.1	This study
	HH-2	0.715509 (5)	0.512062 (7)	− 11.2	
	HH-3	0.715225 (5)	0.512040 (6)	− 11.7	
	HH-4	0.715271 (5)	0.512007 (5)	− 12.3	
	HH-5	0.715585 (5)	0.511988 (8)	− 12.7	
Changjiang Bedload	CJ-1	0.713292 (8)	0.512058 (6)	− 11.3	
	CJ-2	0.717302 (5)	0.512054 (6)	− 11.4	
	CJ-3	0.718292 (5)	0.512045 (5)	− 11.6	
Old Huanghe Bedload	OH-1	0.713682 (7)	0.512098 (5)	− 10.5	
	OH-2	0.713592 (7)	0.512046 (7)	− 11.5	
	OH-3	0.714419 (5)	0.512010 (3)	− 12.3	
	OH-4	0.715289 (6)	0.512035 (9)	− 11.8	
	OH-5	0.716186 (7)	0.511968 (8)	− 13.1	
Huanghe Bedload (n = 8)		0.71736 ± 0.00033		− 13.3 ± 1.4	Rao et al. (2017)
Huanghe Suspended (n = 21)		0.72150 ± 0.00133		− 11.8 ± 0.2	Hu et al., unpublished data
Old Huanghe (n = 8)		0.71861 ± 0.00098		− 11.9 ± 0.4	Rao et al. (2017)
Changjiang Bedload (n = 9)		0.71857 ± 0.00149		− 11.9 ± 0.3	Rao et al. (2017)
Changjiang Suspended (n = 45)		0.72598 ± 0.00526		− 11.8 ± 1.1	Yang et al. (2007a), Mao et al. (2011), Luo et al. (2012)

yielding a mean value of 0.512120 ± 8 (2σ) (N = 12) for $^{143}Nd/^{144}Nd$. For convenience, the $^{143}Nd/^{144}Nd$ ratio is expressed as εNd with the Chondritic Uniform Reservoir value of 0.512638 (Jacobsen and Wasserburg, 1980).

4. Results and discussion

4.1. Sr–Nd isotopic compositions of Core YSC-1 and riverine sediments

In the marine environment, the original isotopic feature of detrital fraction may be largely disturbed by the biogenic, organic, and authigenic components in the sediments, which have been effectively removed before geochemical analysis in this study. Consequently, the sediment isotopic compositions obtained in this study mainly reflect those of the detrital fraction. The Sr–Nd isotopic compositions of Core YSC-1 are shown in Fig. 3 and Table 1. $^{87}Sr/^{86}Sr$ ratios of Core YSC-1 range from 0.717462 to 0.719291, with an average value of 0.718406. $^{143}Nd/^{144}Nd$ values of Core YSC-1 vary between 0.511926 and 0.512016, corresponding εNd ranging from − 13.9 to − 12.1. $^{87}Sr/^{86}Sr$ ratios and εNd values of the Huanghe, the Old Huanghe, and the Changjiang riverine sediments are comparable with each other, with average values of 0.71536 ± 0.0018, 0.71463 ± 0.0110, and 0.71630 ± 0.00265 and − 12.0 ± 0.56, − 11.8 ± 0.93, and − 11.4 ± 0.50, respectively (Table 2).

Sr isotopes generally increased with decreasing grain size, resulting from more clay minerals and micas with high Rb/Sr and $^{87}Sr/^{86}Sr$ ratios enriched in the finer sediments (Tütken et al., 2002; Meyer et al., 2011; Garçon et al., 2014). However, we did not observe the $^{87}Sr/^{86}Sr$-mean grain size (Mz) negative relationship in our data set (Fig. 4a), suggesting the grain size effect on $^{87}Sr/^{86}Sr$ ratios may be secondary. Additionally, sediments from Core YSC-1 lie along a relatively well-defined linear array (r^2 = 0.56, p < 0.001) in $^{87}Sr/^{86}Sr$ vs. 1/Sr plot, and first order variations along this trend indicate binary mixing from two different sources with contrast Sr concentrations and isotope ratios (Fig. 4b). Interestingly, a significant correlation exists between εNd and Mz, with less radiogenic Nd isotopic compositions in the coarse sediment (Fig. 5a). It is often assumed that there is no significant dependence of εNd on grain size or chemical weathering (Tütken et al., 2002; Meyer et al., 2011; Garçon et al., 2014; Bayon et al., 2015). This significant correlation between εNd and Mz most likely related to

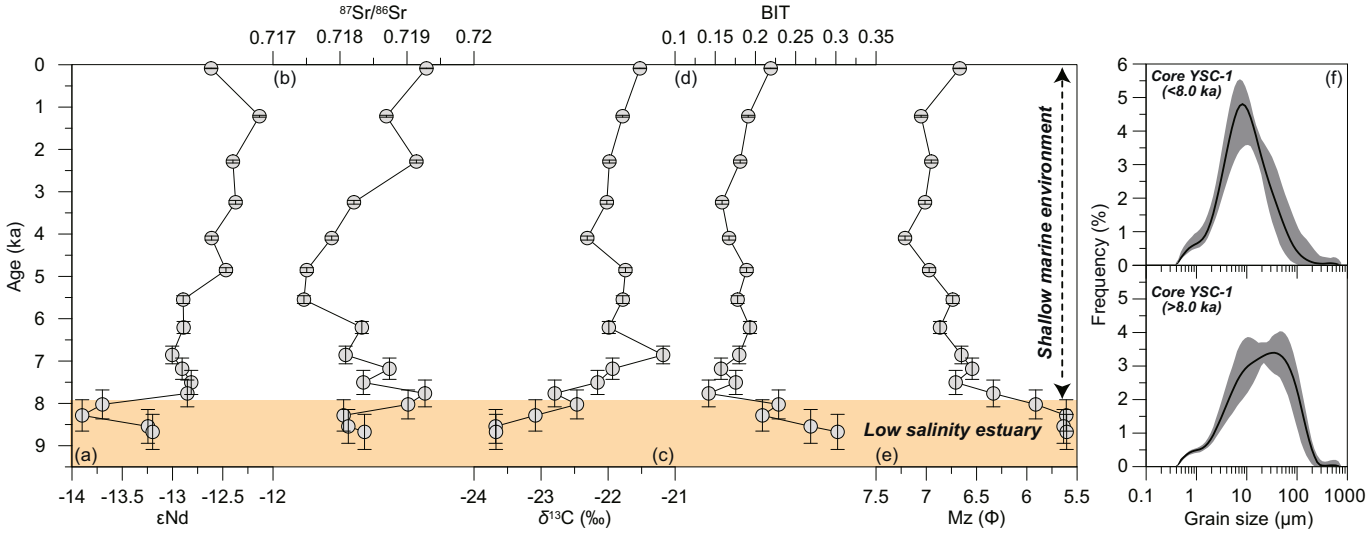

Fig. 3. Downcore variations of εNd values (a), $^{87}Sr/^{86}Sr$ ratios (b), $\delta^{13}C$ of sedimentary organic matters (c), BIT values (d) (Ge et al., 2014), and mean grain size (e) of Core YSC-1 in the South Yellow Sea. Grain size distributions of bulk samples from Core YCS-1 are also shown (f). The grain size frequency curves of Core YSC-1 (< 8.0 ka) display a unimodal pattern with a narrow range of mean grain size (8–12 μm). Core YSC-1 before ~8 ka is characterized by coarser grain size, lower $\delta^{13}C$ values, and higher BIT values, indicating the study area was highly influenced by fresh-water and terrigenous materials at that time. (For interpretation of the references to colour in this figure legend, the reader is referred to the web version of this article.)

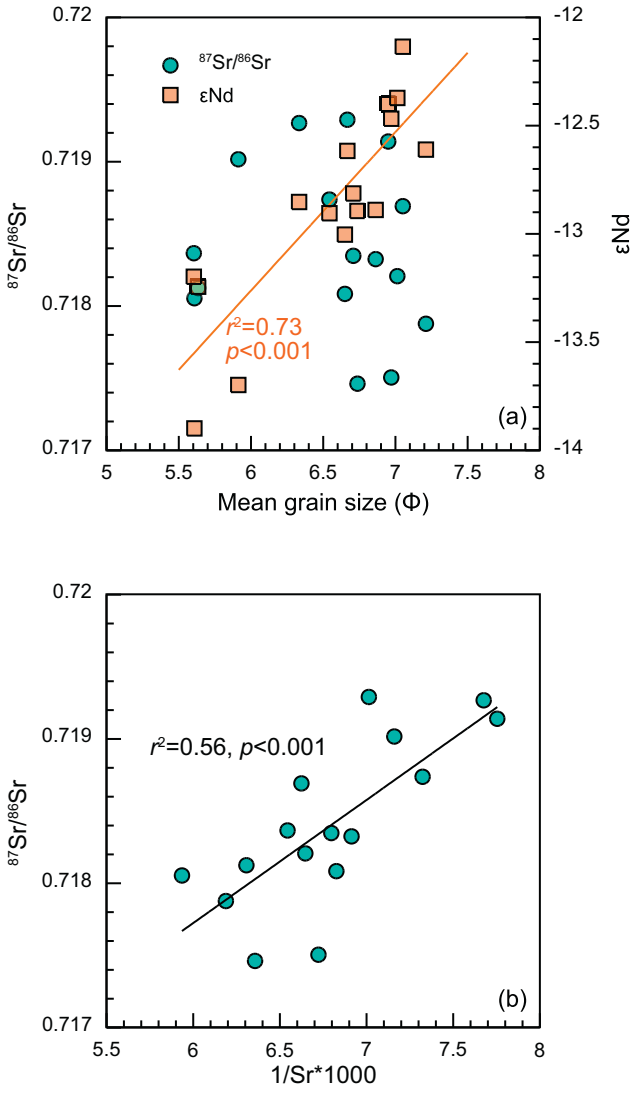

Fig. 4. (a) Correlations between $^{87}Sr/^{86}Sr$ ratios (εNd) and mean grain size and (b) Correlations between $^{87}Sr/^{86}Sr$ ratios and 1/Sr * 1000.

sediment provenance, suggesting there are variable contributions of detritus to individual sediments from distinctly different grain size fractions. Such variations of εNd in different size fractions of bulk sample have been reported in previous studies, which is ascribed to different sediment-transport mechanism such as riverine suspended sediment and eolian dust (Innocent et al., 2000; Révillon et al., 2011).

Recent studies have indicated riverine suspended sediments always having more radiogenic $^{87}Sr/^{86}Sr$ than that of bedload sediments, resulting from higher proportion of Sr-radiogenic minerals (e.g., clay, micas) in the former whereas more Sr-unradiogenic minerals (e.g., epidote, plagioclase) in the latter (Bouchez et al., 2011; Luo et al., 2012; Garçon et al., 2014). This is also found in the Changjiang and Huanghe basins, $^{87}Sr/^{86}Sr$ ratios in the Changjiang and Huanghe suspended sediments are 0.7275 ± 0.053 (Mao et al., 2011; Luo et al., 2012) and 0.7215 ± 0.014 (Hu et al., unpublished data), respectively, which are obviously higher than that of bedloads (0.7163 ± 0.026 in the Changjiang and 0.7154 ± 0.002 in the Huanghe) (Table 2). Lim et al. (2015a) indicated that Sr isotopic composition in both Chinese and Korean riverine sediments was a function of grain size, with higher $^{87}Sr/^{86}Sr$ in clay-dominated fractions than that of silt-dominated. The large variations of $^{87}Sr/^{86}Sr$ ratios in the Chinese and Korean riverine sediments lead them to overlap each other (i.e., not distinctive enough),

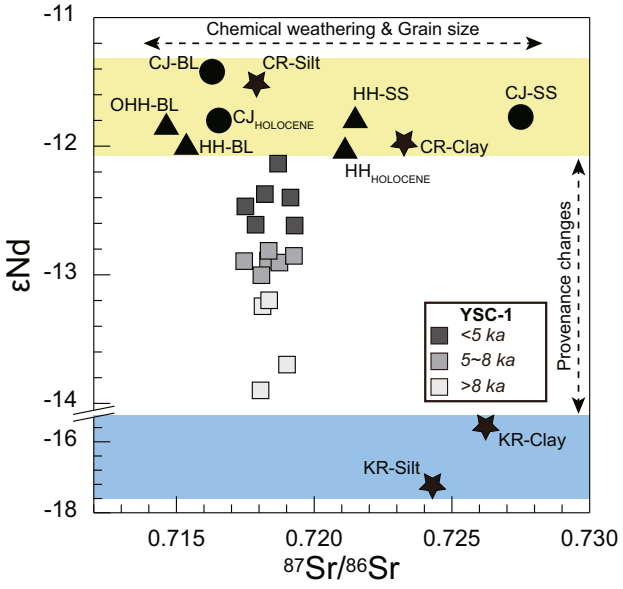

Fig. 5. Plot of εNd vs. $^{87}Sr/^{86}Sr$ for the samples of Core YSC-1 and riverine sediments. Changjiang suspended sediment (CJ-SS) data from Yang et al. (2007a) and Mao et al. (2011); Korean rivers (KR) and Chinese rivers (CR) silt and clay fractions data from Lim et al. (2015a); Sr–Nd isotopes of the Holocene sediments from the Changjiang Estuary ($CJ_{HOLOCENE}$) (Bi et al., 2017) and Huanghe Delta ($HH_{HOLOCENE}$) (Hu et al., 2012a) are also shown. Changjiang, Huanghe, and Old Huanghe bedload (CJ-BL, HH-BL, and OHH-BL) data are measured in this study. $^{87}Sr/^{86}Sr$ ratios in both Chinese and Korean riverine sediments was a function of grain size, whereas εNd values of the Changjiang and Huanghe sediments are unaffected by mineral sorting.

and thus it might not be an appropriate provenance tracer in the Yellow Sea (Table 2 and Fig. 5).

For the εNd values, the offsets between the suspended and bedload of Changjiang and Huanghe (including the Old Huanghe) are within ~0.5 εNd units (Table 2 and Fig. 5), suggesting εNd of these two large river basins appears unaffected by mineral sorting. Similar results have been reported by Bayon et al. (2015) and Lim et al. (2015a), the Changjiang and Huanghe sediments display similar Nd isotopic signatures in both clay and silt fractions. Though Nd isotopic compositions of Korean riverine sediments exhibit variations between the silt-dominated (−17.2 ± 1.3) and clay-dominated fractions (−15.6 ± 1.4), they are generally less radiogenic compared to the Changjiang and Huanghe, mainly reflecting inherited signatures of their source rocks (Lim et al., 2015a). Shifts in the intensity and pattern of monsoonal precipitation have changed Nd isotopic composition of the Huanghe sediments on glacial-interglacial timescales, with less εNd values (−14.5 to −12.6) during the Marine Isotope Stage 2 (MIS 2) than those of Holocene (−12.3 to −11.9) (Hu et al., 2012a). In contrast, Nd isotopic compositions of the Changjiang sediments show no obvious discrepancy between the modern Changjiang sediments and those of MIS 2 (Yang et al., 2007b). Most recently, Bi et al. (2017) presented new Sr–Nd isotopic records of Core CM97 in the Changjiang Estuary, with εNd values varied from −12.5 to −10.8 (averaged εNd = −11.8 ± 0.4) during the Holocene and from −12.1 to −10.7 (averaged εNd = −11.5 ± 0.5) during the late glacial period. Nevertheless, Holocene Nd isotopic compositions of these two large rivers fall well within the range of their present-day endmembers (Fig. 5). As discussed above, Nd isotopes are not significantly fractionated during the erosion/transport processes, and are therefore robust proxies for tracing the Holocene sediment inputs from the Chinese and Korean rivers (Fig. 5).

4.2. Sediment sources discrimination of the Central Yellow Sea Mud and paleoenvironmental implications

The reliable interpretation of sediment provenance requires knowledge of different potential source areas and end-members. The East China Sea Shelf was subaerially exposed during the LGM (26.5–19 ka), when the global sea level was about 120–135 m below present sea level (b.p.s.l.) (Clark et al., 2009). The paleo-Changjiang and paleo-Huanghe might flow across the East China Sea Shelf and their river mouths located closer to the present day's outer shelf at that time (Yang et al., 2014). As the postglacial seal level rapid rising, the tidal-current regime in the Yellow Sea has been significantly modified due to the changed coastline configuration until ~9 ka (sea level reached to 15 m b.p.s.l.) (Uehara and Saito, 2003). Since then, the tidal field of Yellow Sea became very similar with present situation, seabed erosional materials under circumstances of weak bottom stress (< 0.35 N/m^2) should be insignificant. Therefore, sediments deposited on the CYSM consist mainly of erosion products of the nearby continental areas transported by river and/or eolian dust. However, Qiao et al. (2017) recently indicated that atmospheric deposition at centennial timescale only contributed 1–2% of the total burial sediment in the Yellow Sea mud areas. Indeed, the East China Seas, as a typical river-dominated marginal sea, received a large volume of fluvial sediments from the adjacent continent during the Holocene, whereas the eolian dust's influence should be insignificant (Hu et al., 2014), thus we do not consider and discuss the dust contribution in the following sections.

Due to high smectite contents of the Huanghe sediments in comparison with other possible sources, the smectite/illite ratio has been regarded as a suitable proxy for distinguishing the Huanghe provenance (Li et al., 2014b; Lim et al., 2015b). Using the smectite/illite ratio as an additional constraint, we propose a simple scenario to explain sediment provenances of the CYSM by a three-endmembers mixing model of (1) high smectite/illite ratio and high εNd values of the Huanghe, (2) intermediate smectite/illite ratio and high εNd values of the Changjiang, and (3) low smectite/illite ratio and low εNd of the Korean small rivers (Fig. 6a). Samples before ~8 ka are located at the mixing line between the Huanghe and Korean riverine endmembers, whereas samples after ~8 ka are mostly scattered around the mixing line between the Changjiang and Korean riverine endmembers (Fig. 6a). Due to the large variability of smectite/illite ratios of these three endmembers, we have to concentrate on Nd isotopic system to quantify the proportion of Huanghe (before 8 ka) and Changjiang (after 8 ka) sediments (Fig. 6b), respectively. Nd isotopes were selected to do this because (1) it is not significantly fractionated during the erosion/transport processes as discussed above, and (2) a large set of samples from the Huanghe and Changjiang have been measured for Nd isotopic compositions falling within a narrow range (Table 2). Additionally, Nd isotopic compositions of Korean riverine sediments show much more variability (Lim et al., 2015a), therefore two different low εNd endmembers with constant Nd concentration for Korean riverine sediments are used for mixing calculations (Fig. 6b). Results show that the Huanghe is the major sediment contributor (71% to 82%) to the CYSM before ~8 ka, whereas the Changjiang has become the predominant sediment source (77% to 84%) over the past ~8 kyr.

Traditionally, the δ^{13}C and branched vs. isoprenoidal tetraether (BIT) index of sedimentary organic matter are used to determine the sources of organic matter. Terrestrial organic matter usually has δ^{13}C values that are more negative (about − 27‰) than marine organic matter (− 20‰) (Meyers, 1997), whereas the BIT was found to be close to 1 (0.90 ± 0.14, n = 224) for soil organic matter, close to 0 (0.04 ± 0.03, n = 278) for marine organic matter (Schouten et al., 2013). Before ~8 ka, Core YSC-1 was characterized by coarser grain size, lower δ^{13}C values (Zou et al., 2017), and higher BIT values (Ge et al., 2014) (Fig. 3). These indicated the study area at that time was highly influenced by fresh-water and terrigenous materials, consistent with a low salinity estuary environment defined by previous studies

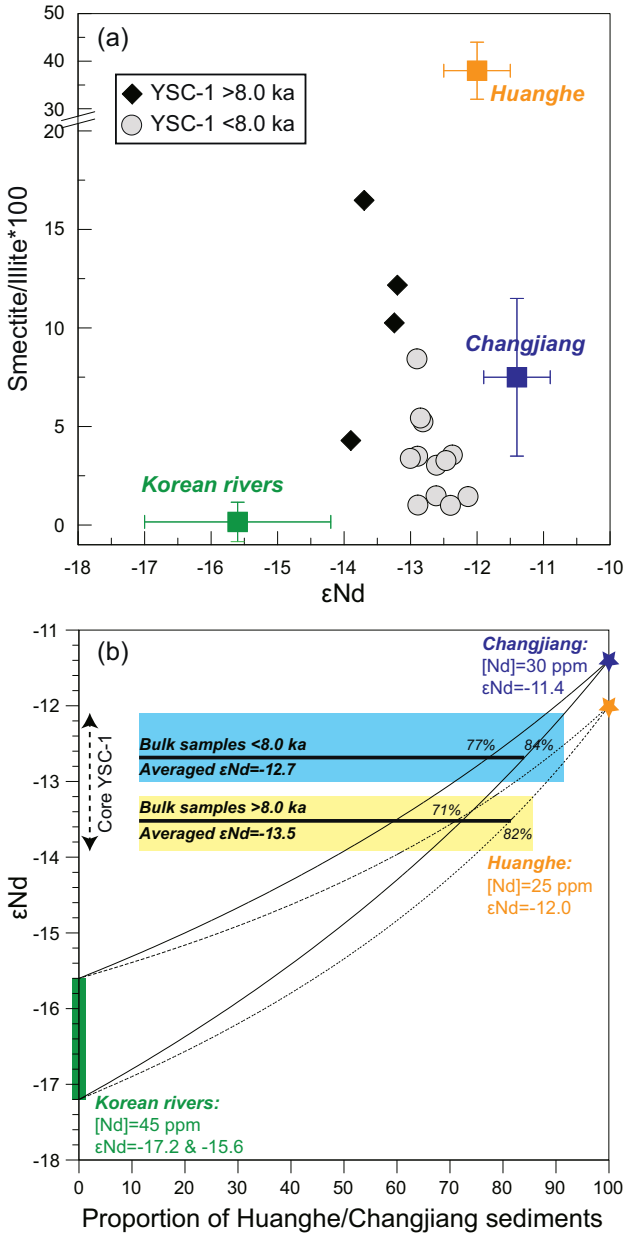

Fig. 6. (a) Three-endmembers mixing model for the South Yellow Sea based on εNd and smectite/illite ratios. Clay minerals data from Li et al. (2014b). (b) Calculated Nd isotopic compositions of Core YSC-1 mixed by the Huanghe (> 8.0 ka)/the Changjiang (< 8.0 ka) and Korean rivers. (For interpretation of the references to colour in this figure legend, the reader is referred to the web version of this article.)

(Kim and Kennett, 1998; Kim and Kucera, 2000; Xiang et al., 2008). In contrast, Core YSC-1 after ~8.0 ka, with finer grain size, higher δ^{13}C values, and lower BIT values, was interpreted to be formed in a shallow shelf environment since the sea level approximated its highstand (Fig. 3). The paleo-Huanghe was deduced to empty into the Bohai Strait and formed the proximal Huanghe subaqueous delta along the northern shore of the Shandong Peninsula at 11.6–9.6 ka (Xue et al., 2004; Liu et al., 2007a). However, it has frequently shifted its lower course north-southward and formed a subaqueous deltaic deposit in the offshore area of southern Yellow Sea during the period of 9.6–8.5 ka (Xue et al., 2004), as well as eight superlobes in the western plain of Bohai Sea since 7.8–8.2 ka (Saito et al., 2000). Based on Nd isotopes and clay minerals results, we infer that the paleo-Huanghe mouth and/or its subaqueous delta was located proximal to the study area before ~8.0 ka. Abrupt decrease of the Huanghe sediments to Core YSC-1 at

~8.0 ka is likely a direct response to the northward shift of paleo-Huanghe. Since then, the Huanghe sediments' influence on the CYSM is minor due to the sediment trapping effect of winter oceanic fronts along the northern side of Shandong Peninsula (Hu et al., 2011; Li et al., 2014b; Li et al., 2016).

The dominant contribution of Changjiang sediments to the CYSM since ~8.0 ka may be closely linked to the formation of Changjiang Delta after the rapid sea level rise during 9–8 ka (Hori et al., 2002). Although the Changjiang sediments were largely trapped within the incised valley during the initial aggradation stage (Hori et al., 2002; Song et al., 2013), some of the Changjiang sediments could be transported southward by the East China Sea Coastal Current (ECSCC) and formed an elongated (~1000 km) distal subaqueous mud wedge in the inner shelf of East China Sea (Xu et al., 2012), as well as northeastward to the CYSM via the summer Changjiang Diluted Water (CDW) (Li et al., 2016). When the sea level kept stable after 6–5 ka, depocenters of the Changjiang Delta gradually moved seaward and formed a series of seaward migrating river-mouth sand bars from Zhenjiang to the present river mouth (Hori et al., 2002; Song et al., 2013), meanwhile more sediments may be escaped from the Changjiang deltaic/estuarine systems. In the other hand, the modern YSWC is deduced to be formed at 6–5 ka (Xiang et al., 2008; Li et al., 2009; Wang et al., 2014; Nan et al., 2017), the concomitant winter oceanic fronts likely prevent most of the Korean riverine sediments from spreading into the CYSM since then (Hu et al., 2011, Li et al., 2014b). This is consistent with the slightly increased contribution of Changjiang sediments in Core YSC-1 since ~5 ka. In summary, the stepwise increasing of εNd values of Core YSC-1, together with the decreasing smectite/illite ratios, reveal distinct changes in sediment supplies from adjacent rivers and regional marine circulation over the Holocene.

4.3. $^{87}Sr/^{86}Sr$ ratios tracing changes in the erosion patterns on the Changjiang Basin?

Sr isotope composition of detrital sediments is predominantly controlled by source heterogeneity, mineral sorting (grain size effect) during the transport processes, and chemical weathering intensity on continent. In marked contrast to the minor changes recorded by εNd values since ~8 ka (−13 to −12.1) (i.e., the dominant Changjiang source), $^{87}Sr/^{86}Sr$ ratios of Core YSC-1 document relatively large variations (Fig. 7). Hydrodynamic sorting does not appear to have significant influence on the $^{87}Sr/^{86}Sr$ ratios of Core YSC-1, as indicated by poor correlation between $^{87}Sr/^{86}Sr$ ratios and mean grain size (Fig. 4a). In fact, the Changjiang source-to-sink processes display seasonal variability both in temporal and spatial. The southward transport process mainly occurred in winter-half-years, when the previously deposited sediments from the Changjiang estuary/subaqueous delta are readily resuspended by strong wind-induced waves, and transported along the inner shelf via strong East China Sea Coastal Current (Fig. 1) (Liu et al., 2007b; Xu et al., 2012). Hydrodynamic sorting effects play an important role during this multi cycle of resuspended-transport-deposition processes, as recently indicated by Bi et al. (2017). In comparison, the northeastward dispersal of Changjiang sediments mostly happened during the flood season (May to September) by direct diffusion effect of the CDW (Pang et al., 2011; Li et al., 2016). Once the Changjiang suspended sediment reached the CYSM area, where the YSCWM occupied, it can be trapped by this cold water mass due to strong water column stratification and weak tidal and residual currents (Li et al., 2016). Wang et al. (2014) also indicated that the formation of CYSM is not related directly to the YSWC, which only changed the sediment properties of mud deposits, whereas cold water mass developed in this area is important as it helps to trap more fine-grained particles. After ~8.0 ka, the grain size frequency curves of Core YSC-1 displays a unimodal pattern with a narrow range of Mz (8–12 μm) (Fig. 3f), suggesting that sediments of Core YSC-1 might be mainly derived from one predominant source. This further confirms that the summertime diffusion of Changjiang sediments may be a continuous and stable process during the last 8.0 ka.

Radiogenic Sr is preferentially released to solution and removed from the source region during the chemical weathering, resulting from the early breakdown of high Rb/Sr minerals (e.g., mica and K-feldspar). Consequently, when the effects of mineral sorting and source heterogeneity are reliable excluded, variations of $^{87}Sr/^{86}Sr$ ratios in marine sediments likely reflect changes in continental weathering regimes. For example, Sr isotope variations of Core 905P in the Arabian Sea mainly reflect the relative importance of physical versus chemical weathering, with low Sr isotopes indicating increased chemical weathering intensity associated with increased monsoonal precipitation and vice versa (Jung et al., 2004). Another study of marine sediments from the Bay of Bengal and the Andaman Sea indicated that wet periods of summer monsoon reinforcement correspond to an increase in weathering of the Irrawaddy plain soils and a decrease of $^{87}Sr/^{86}Sr$ ratio at glacial–interglacial timescales (Colin et al., 2006). Using Sr–Nd isotopes in two size fractions of five sediment cores from offshore NW Africa, Meyer et al. (2011) suggested that variations in Sr isotope ratios are related to a latitudinal shift of the northern limit of the African rain belt and associated wind systems, which in turn changed the humidity and rate of chemical weathering over NW Africa. Most recently, Ali et al. (2015) also found high smectite/(illite + chlorite) ratios and low $^{87}Sr/^{86}Sr$ ratios of Core NGHP Site 17 in the Andaman Sea during the Holocene, indicating enhanced chemical weathering and a stronger South Asian monsoon compared to MIS 2 and MIS 3. However, $^{87}Sr/^{86}Sr$ ratios of Core YSC-1 co-varied with CIA and Rb/Sr ratios during the last ~8 kyr (Fig. 7). This is opposite to the expectation that low $^{87}Sr/^{86}Sr$ ratios corresponding to the intensified chemical weathering (i.e., high CIA values and Rb/Sr ratios). Thus, we cannot attribute our $^{87}Sr/^{86}Sr$ data to fractionation during chemical weathering within the Changjiang basin.

An alternative explanation arises when the spatial difference of geological and climatic settings within the Changjiang basin is considered. Geologically, the Changjiang basin consists of variable strata from the Archean to the Quaternary period, resulting in variable Sr isotopic compositions in the Changjiang sediments (Yang et al., 2007a; He et al., 2015). Erosions of Emeishan Basalts and younger igneous rocks produced low $^{87}Sr/^{86}Sr$ in sediments derived from the upper reaches, whereas more radiogenic Sr isotopes occurred in the middle-lower reaches due to wide outcrops of old metamorphic rocks (Yang et al., 2007a; He et al., 2015). In the other hand, the average CIA values increased from the upper to middle-lower reaches, due to the relative flat topography and warm/wet climate within the middle-lower Changjiang Basin (Shao and Yang, 2012; He et al., 2015). Seasonal variations of $^{87}Sr/^{86}Sr$ and CIA values of the Changjiang suspended sediments are primarily controlled by changed provenance associated with the NE-SW shift of rainbelt, the relative decrease in $^{87}Sr/^{86}Sr$ ratios and CIA values during the flood season primarily reflect enhanced physical erosion in the upper basin (Shao and Yang, 2012; He et al., 2015). Therefore, we speculate that spatial varying rainfall intensities on sub-basin scales have modified sediment exports from different parts of the Changjiang Basin at millennial timescales. Indeed, significant impacts of long-term climate changes on the erosion/weathering patterns within large river basins have been well documented (Rahaman et al., 2009; Box et al., 2011; Hu et al., 2012a; Blanchet et al., 2013; Woodward et al., 2015). $^{87}Sr/^{86}Sr$, CIA, and Rb/Sr ratios of Core YSC-1 indicated that the relative contribution of sediments derived from the upper Changjiang gradually increased from ~8 ka, reached a maximum between 6 and 3 ka, and then gradually decreased to the present level (Fig. 7b-d).

Climatically, the Indian Summer Monsoon (ISM) is the dominant contributor of rainfall in the upper reaches, whereas the East Asian Summer Monsoon (EASM) is the major precipitation source in the middle-lower reaches of Changjiang (Wang et al., 2008). The Holocene paleo-humidity of the ISM region, with no significant spatial

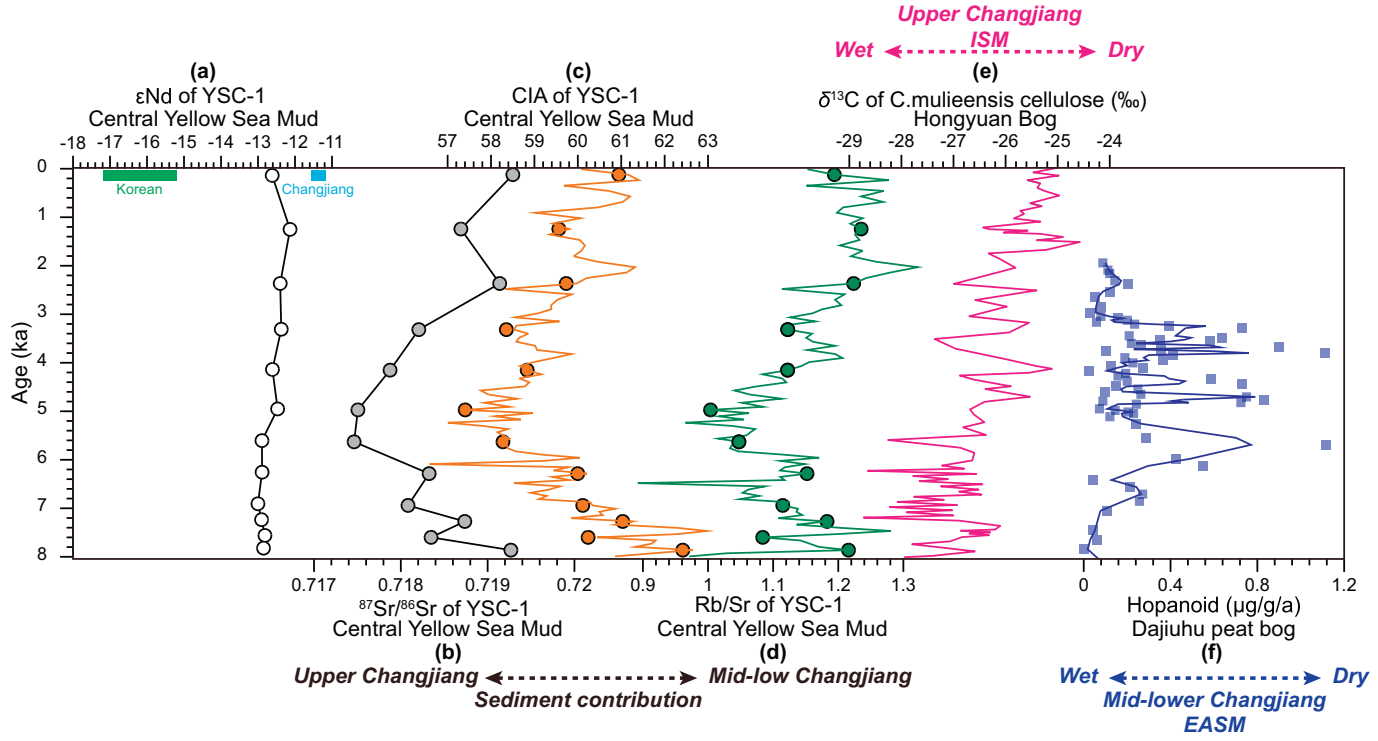

Fig. 7. Downcore variations of εNd (a), $^{87}Sr/^{86}Sr$ (b), CIA (c), and Rb/Sr (d) ratios of Core YSC-1 since ~8 ka. (e) $\delta^{13}C$ of C. mulieensis cellulose (‰) from the Hongyuan Bog (Hong et al., 2003) indicating the Indian Summer Monsoon in the upper Changjiang basin, and (f) Hopanoid (μg/g/a) in the Dajiuhu Peat Bog (Xie et al., 2013) indicating the East Asian Summer Monsoon in the mid-lower Changjiang basin.

differences, was overall humid during the Early-Holocene and early Mid-Holocene (ca. 11–6 ka) and then weakened towards the Late-Holocene (Hong et al., 2003; Rao et al., 2016) (Fig. 7e). In contrast, the Holocene paleo-humidity of EASM region display clear spatial differences, with a spatial "− + −" mode during the Early-Holocene and Late-Holocene, but a spatial "+ − +" mode during the Mid-Holocene for the southern, central, and northern China, respectively (Rao et al., 2016). These spatial precipitation differences of the Holocene EASM may be related to coupled variations in the west-east Equatorial Pacific thermal gradient and the location of the West Pacific Subtropical High (WPSH) (Rao et al., 2016). Specifically, the Dajiuhu peat bog and Heshang stalagmite demonstrate that precipitation decreased and climate became more arid in the middle reaches of Changjiang during the Mid-Holocene, and that precipitation increased and climate became more humid during the Late-Holocene (Xie et al., 2013) (Fig. 7f). Paleoclimate Modeling Intercomparison Project (PMIP) simulations also demonstrate that the middle and lower reaches of Changjiang became more arid during the Mid-Holocene (Jiang et al., 2013). Temporal variations of the relative sediment contributions from the different subbasins in the Changjiang watershed coincide generally with the asynchronous evolution of monsoon precipitation in the upper (ISM) and middle-lower Changjiang (EASM) during the last ~8 kyr (Fig. 7e-f). Our results seem to be different from that of Bi et al. (2017), thus more researches are necessary to reveal the detailed information of monsoon-climate influences on the Changjiang basin, as well as the complex source-to-sink processes from the upland to the marginal seas.

5. Conclusions

Sr–Nd isotopic signatures of Core YSC-1 are used to decipher terrigenous sediment provenances and transport mechanisms in the South Yellow Sea during the Holocene. $^{87}Sr/^{86}Sr$ ratios of Core YSC-1 vary from 0.717462 to 0.719291, with an average value of 0.718406. εNd values of Core YSC-1 vary between − 13.9 and − 12.1. $^{87}Sr/^{86}Sr$ ratios may be not appropriate provenance tracer in this study area, due to the large variations of $^{87}Sr/^{86}Sr$ ratios in the Chinese and Korean riverine sediments. In contrast, Nd isotopic compositions are not significantly fractionated during the erosion/transport processes, and therefore are robust proxies for tracing the Holocene sediment inputs from the Chinese and Korean rivers. Combined with clay minerals results, a three-endmembers mixing model (i.e., the Changjiang, Huanghe, and Korean rivers) is proposed to explain the sediment provenances in the Central Yellow Sea Mud. Two stepwise increasing of εNd values of Core YSC-1, together with the decreasing smectite/illite ratio, reveals distinct changes in sediment supplies from adjacent rivers and regional marine circulation during the Holocene. The Huanghe is the major sediment contributor to the study area before ~8 ka, whereas the Changjiang have become the predominant sediment source over the past 8 kyr. In addition, we attributed variations in $^{87}Sr/^{86}Sr$ ratios, as well as CIA and Rb/Sr ratios, of Core YSC-1 since ~8 ka to changes in the erosion patterns on the Changjiang basin, which in turn is associated with the asynchronous evolution of monsoon precipitation in the upper (ISM) and middle-lower Changjiang (EASM).

Acknowledgments

We sincerely appreciate the constructive and stimulating comments by Editor Jerome Gaillardet and two anonymous referees that helped to greatly improve this paper. This study was jointly supported by the National Natural Science Foundation of China (41476052, 41576058, and 41522305), the Security Project of Marine Geology (GHZ201200510), the Open Foundation of the State Key Laboratory of Loess and Quaternary Geology (SKLLQG1707), and the Shandong Provincial Natural Science Foundation of China (ZR2016DM08).

References

Alexander, C., DeMaster, D., Nittrouer, C., 1991. Sediment accumulation in a modern epicontinental-shelf setting: the Yellow Sea. Mar. Geol. 98, 51–72.
Ali, S., Hathorne, E.C., Frank, M., Gebregiorgis, D., Stattegger, K., Stumpf, R., Kutterolf,

S., Johnson, J.E., Giosan, L., 2015. South Asian monsoon history over the past 60 kyr recorded by radiogenic isotopes and clay mineral assemblages in the Andaman Sea. Geochem. Geophys. Geosyst. 16, 1525–2027.
Bayon, G., Toucanne, S., Skonieczny, C., André, L., Bermell, S., Cheron, S., Dennielou, B., Etoubleau, J., Freslon, N., Gauchery, T., Germain, Y., Jorry, S.J., Ménot, G., Monin, L., Ponzevera, E., Rouget, M.L., Tachikawa, K., Barrat, J.A., 2015. Rare earth elements and neodymium isotopes in world river sediments revisited. Geochim. Cosmochim. Acta 170, 17–38.
Bi, L., Yang, S., Zhao, Y., Wang, Z., Dou, Y., Li, C., Zheng, H., 2017. Provenance study of the Holocene sediments in the Changjiang (Yangtze River) estuary and inner shelf of the East China sea. Quat. Int. 441, 147–161.
Blaauw, M., 2010. Methods and code for 'classical' age-modelling of radiocarbon sequences. Quat. Geochronol. 5, 512–518.
Blanchet, C.L., Tjallingii, R., Frank, M., Lorenzen, J., Reitz, A., Brown, K., Feseker, T., Brückmann, W., 2013. High- and low-latitude forcing of the Nile River regime during the Holocene inferred from laminated sediments of the Nile deep-sea fan. Earth Planet. Sci. Lett. 364, 98–110.
Bouchez, J., Gaillardet, J., France-Lanord, C., Maurice, L., Dutra-Maia, P., 2011. Grain size control of river suspended sediment geochemistry: clues from Amazon River depth profiles. Geochem. Geophys. Geosyst. 12, Q03008.
Box, M.R., Krom, M.D., Cliff, R.A., Bar-Matthews, M., Almogi-Labin, A., Ayalon, A., Paterne, M., 2011. Response of the Nile and its catchment to millennial-scale climatic change since the LGM from Sr isotopes and major elements of East Mediterranean sediments. Quat. Sci. Rev. 30, 431–442.
Clark, P.U., Dyke, A.S., Shakun, J.D., Carlson, A.E., Clark, J., Wohlfarth, B., Mitrovica, J.X., Hostetler, S.W., McCabe, A.M., 2009. The last glacial maximum. Science 325, 710–714.
Clift, P.D., 2010. Enhanced global continental erosion and exhumation driven by Oligo-Miocene climate change. Geophys. Res. Lett. 37, L09402.
Clift, P.D., Hodges, K.V., Heslop, D., Hannigan, R., Van Long, H., Calves, G., 2008. Correlation of Himalayan exhumation rates and Asian monsoon intensity. Nat. Geosci. 1, 875–880.
Cogez, A., Meynadier, L., Allègre, C., Limmois, D., Herman, F., Gaillardet, J., 2015. Constraints on the role of tectonic and climate on erosion revealed by two time series analysis of marine cores around New Zealand. Earth Planet. Sci. Lett. 410, 174–185.
Cole, J., Goldstein, S., Demenocal, P., Hemming, S., Grousset, F., 2009. Contrasting compositions of Saharan dust in the eastern Atlantic Ocean during the last deglaciation and African Humid Period. Earth Planet. Sci. Lett. 278, 257–266.
Colin, C., Turpin, L., Blamart, D., Frank, N., Kissel, C., Duchamp, S., 2006. Evolution of weathering patterns in the Indo-Burman ranges over the last 280 kyr: effects of sediment provenance on 87Sr/86Sr ratios tracer. Geochem. Geophys. Geosyst. 7, Q03007.
Covault, J.A., Fildani, A., 2014. Chapter 23 continental shelves as sediment capacitors or conveyors: source-to-sink insights from the tectonically active Oceanside shelf, southern California, USA. Geol. Soc. Lond. Mem. 41, 315–326.
Covault, J.A., Romans, B.W., Graham, S.A., Fildani, A., Hilley, G.E., 2011. Terrestrial source to deep-sea sink sediment budgets at high and low sea levels: insights from tectonically active Southern California. Geology 39, 619–622.
Dou, Y., Yang, S., Liu, Z., Shi, X., Li, J., Yu, H., Berne, S., 2012. Sr–Nd isotopic constraints on terrigenous sediment provenances and Kuroshio current variability in the Okinawa Trough during the late Quaternary. Palaeogeogr. Palaeoclimatol. Palaeoecol. 365-366, 38–47.
Dou, Y., Yang, S., Shi, X., Clift, P.D., Liu, S., Liu, J., Li, C., Bi, L., Zhao, Y., 2016. Provenance weathering and erosion records in southern Okinawa Trough sediments since 28 ka: geochemical and Sr–Nd–Pb isotopic evidences. Chem. Geol. 425, 93–109.
Frank, M., 2002. Radiogenic isotopes: tracers of past ocean circulation and erosional input. Rev. Geophys. 40, 1–38.
Garçon, M., Chauvel, C., France-Lanord, C., Limonta, M., Garzanti, E., 2014. Which minerals control the Nd–Hf–Sr–Pb isotopic compositions of river sediments? Chem. Geol. 364, 42–55.
Ge, H., Zhang, C.L., Li, J., Versteegh, G.J.M., Hu, B., Zhao, J., Dong, L., 2014. Tetraether lipids from the southern Yellow Sea of China: implications for the variability of East Asia Winter Monsoon in the Holocene. Org. Geochem. 70, 10–19.
Grousset, F.E., Biscaye, P.E., 2005. Tracing dust sources and transport patterns using Sr, Nd and Pb isotopes. Chem. Geol. 222, 149–167.
He, M., Zheng, H., Clift, P.D., Tada, R., Wu, W., Luo, C., 2015. Geochemistry of fine-grained sediments in the Yangtze River and the implications for provenance and chemical weathering in East Asia. Prog. Earth. Planet. Sci. 2, 2–32.
Hong, Y.T., Hong, B., Lin, Q.H., Zhu, Y.X., Shibata, Y., Hirota, M., Uchida, M., Leng, X.T., Jiang, H.B., Xu, H., Wang, H., Yi, L., 2003. Correlation between Indian Ocean summer monsoon and North Atlantic climate during the Holocene. Earth Planet. Sci. Lett. 211, 371–380.
Hori, K., Saito, Y., Zhao, Q., Wang, P., 2002. Evolution of the coastal depositional systems of the Changjiang (Yangtze) River in response to Late Pleistocene-Holocene sea-level changes. J. Sediment. Res. 72, 884–897.
Hu, B., Li, G., Li, J., Yang, M., Wang, L., Bu, R., 2011. Spatial variability of the 210Pb sedimentation rates in the Bohai and Huanghai Seas and its influencing factors. Acta Oceanol. Sin. 33, 125–133.
Hu, B., Li, G., Li, J., Bi, J., Zhao, J., Bu, R., 2012a. Provenance and climate change inferred from Sr–Nd–Pb isotopes of late Quaternary sediments in the Huanghe (Yellow River) Delta, China. Quat. Res. 78, 561–571.
Hu, B., Yang, Z., Zhao, M., Saito, Y., Fan, D., Wang, L., 2012b. Grain size records reveal variability of the East Asian Winter Monsoon since the Middle Holocene in the Central Yellow Sea mud area, China. Sci. China Earth Sci. 55, 1656–1668.
Hu, B., Yang, Z., Qiao, S., Zhao, M., Fan, D., Wang, H., Bi, N., Li, J., 2014. Holocene shifts in riverine fine-grained sediment supply to the East China Sea Distal Mud in response to climate change. The Holocene 24, 1253–1268.
Innocent, C., Fagel, N., Hillaire-Marcel, C., 2000. Sm-Nd isotope systematics in deep-sea sediments: clay-size versus coarser fractions. Mar. Geol. 168, 79–87.
Jacobsen, S.B., Wasserburg, G.J., 1980. Sm-Nd isotopic evolution of chondrites. Earth Planet. Sci. Lett. 50, 139–155.
Jiang, D., Tian, Z., Lang, X., 2013. Mid-Holocene net precipitation changes over China: model–data comparison. Quat. Sci. Rev. 82, 104–120.
Jung, S.J.A., Davies, G.R., Ganssen, G.M., Kroon, D., 2004. Stepwise Holocene aridification in NE Africa deduced from dust-borne radiogenic isotope records. Earth Planet. Sci. Lett. 221, 27–37.
Jung, H.-S., Lim, D., Jeong, D.-H., Xu, Z., Li, T., 2016. Discrimination of sediment provenance in the Yellow Sea: secondary grain-size effect and REE proxy. J. Asian Earth Sci. 123, 78–84.
Kim, J.-M., Kennett, J.P., 1998. Paleoenvironmental changes associated with the Holocene marine transgression, Yellow Sea (Hwanghae). Mar. Micropaleontol. 34, 71–89.
Kim, J.-M., Kucera, M., 2000. Benthic foraminifer record of environmental changes in the Yellow Sea (Hwanghae) during the last 15,000 years. Quat. Sci. Rev. 19, 1067–1085.
Lan, X., Zhang, X., Zhao, G., Zhang, Z., 2009. Dirstributions of rare earth elements in sediments from Core NT1 of the South Yellow Sea and their provenance discrimination. Geochimica 38, 123–132.
Lee, H.J., Chough, S.K., 1989. Sediment distribution, dispersal and budget in the Yellow Sea. Mar. Geol. 87, 195–205.
Li, T., Nan, Q., Jiang, B., Sun, R., Zhang, D., Li, Q., 2009. Formation and evolution of the modern warm current system in the East China Sea and the Yellow Sea since the last deglaciation. Chin. J. Oceanol. Limnol. 27, 237–249.
Li, G., Li, P., Liu, Y., Qiao, L., Ma, Y., Xu, J., Yang, Z., 2014a. Sedimentary system response to the global sea level change in the East China Seas since the last glacial maximum. Earth Sci. Rev. 139, 390–405.
Li, J., Hu, B., Wei, H., Zhao, J., Zou, L., Bai, F., Dou, Y., Wang, L., Fang, X., 2014b. Provenance variations in the Holocene deposits from the southern Yellow Sea: clay mineralogy evidence. Cont. Shelf Res. 90, 41–51.
Li, Y., Li, A.-C., Huang, P., Xu, F.-J., Zheng, X.-F., 2014c. Clay minerals in surface sediment of the north Yellow Sea and their implication to provenance and transportation. Cont. Shelf Res. 90, 33–40.
Li, T., Xu, Z., Lim, D., Chang, F., Wan, S., Jung, H., Choi, J., 2015. Sr–Nd isotopic constraints on detrital sediment provenance and paleoenvironmental change in the northern Okinawa Trough during the Late Quaternary. Palaeogeogr. Palaeoclimatol. Palaeoecol. 430, 74–84.
Li, G., Qiao, L., Dong, P., Ma, Y., Xu, J., Liu, S., Liu, Y., Li, J., Li, P., Ding, D., Wang, N., Olusegun, A.D., Liu, L., 2016. Hydrodynamic condition and suspended sediment diffusion in the Yellow Sea and East China Sea. J. Geophys. Res. Oceans 121, 6204–6222.
Lim, D.I., Jung, H.S., Choi, J.Y., Yang, S., Ahn, K.S., 2006. Geochemical compositions of river and shelf sediments in the Yellow Sea: grain-size normalization and sediment provenance. Cont. Shelf Res. 26, 15–24.
Lim, D., Jung, H.S., Choi, J.Y., 2014. REE partitioning in riverine sediments around the Yellow Sea and its importance in shelf sediment provenance. Mar. Geol. 357, 12–24.
Lim, D., Jung, H., Xu, Z., Jeong, K., Li, T., 2015a. Elemental and Sr–Nd isotopic compositional disparity of riverine sediments around the Yellow Sea: constraints from grain-size and chemical partitioning. Appl. Geochem. 63, 272–281.
Lim, D., Xu, Z., Choi, J., Li, T., Kim, S., 2015b. Holocene changes in detrital sediment supply to the eastern part of the central Yellow Sea and their forcing mechanisms. J. Asian Earth Sci. 105, 18–31.
Liu, J., Saito, Y., Wang, H., Yang, Z., Nakashima, R., 2007a. Sedimentary evolution of the Holocene subaqueous clinoform off the Shandong Peninsula in the Yellow Sea. Mar. Geol. 236, 165–187.
Liu, J.P., Xu, K.H., Li, A.C., Milliman, J.D., Velozzi, D.M., Xiao, S.B., Yang, Z.S., 2007b. Flux and fate of Yangtze River sediment delivered to the East China Sea. Geomorphology 85, 208–224.
Luo, C., Zheng, H., Wu, W., Wang, P., Chen, Y., Wei, X., 2012. Sr-Nd isotope stratification along water depth: an example from Datong hydrological station of Yangtze River. Chin. Sci. Bull. 57, 4482–4490.
Mao, C., Chen, J., Yuan, X., Yang, Z., Ji, J., 2011. Seasonal variations in the Sr-Nd isotopic compositions of suspended particulate matter in the lower Changjiang River: Provenance and erosion constraints. Chin. Sci. Bull. 56, 2371–2378.
McLennan, S., 1993. Weathering and global denudation. J. Geol. 101, 295–303.
Meyer, I., Davies, G.R., Stuut, J.-B.W., 2011. Grain size control on Sr-Nd isotope provenance studies and impact on paleoclimate reconstructions: an example from deep-sea sediments offshore NW Africa. Geochem. Geophys. Geosyst. 12, Q03005.
Meyers, P.A., 1997. Organic geochemical proxies of paleoceanographic, paleolimnologic, and paleoclimatic processes. Org. Geochem. 27, 213–250.
Milliman, J.D., Farnsworth, K.L., 2011. River Discharge to the Coastal Ocean: A Global Synthesis. Cambridge University Press.
Moon, J., Pang, I., Yoon, J., 2009. Response of the Changjiang diluted water around Jeju Island to external forcings: a modeling study of 2002 and 2006. Cont. Shelf Res. 29, 1549–1564.
Nan, Q., Li, T., Chen, J., Chang, F., Yu, X., Xu, Z., Pi, Z., 2017. Holocene paleoenvironment changes in the northern Yellow Sea: evidence from alkenone-derived sea surface temperature. Palaeogeogr. Palaeoclimatol. Palaeoecol. 483, 83–93.
Nesbitt, H.W., Young, G.M., 1982. Early Proterozoic climates and plate motions inferred from major element chemistry of lutites. Nature 299, 715–717.
Pang, C., Yu, W., Yang, Y., Han, D., 2011. An improved method for evaluating the seasonal variability of total suspended sediment flux field in the Yellow and East China Seas. Int. J. Sediment Res. 26, 1–14.
Park, Y.A., Khim, B.K., 1992. Origin and dispersal of recent clay minerals in the Yellow

Sea. Mar. Geol. 104, 205–213.
Qiao, S., Shi, X., Wang, G., Zhou, L., Hu, B., Hu, L., Yang, G., Liu, Y., Yao, Z., Liu, S., 2017. Sediment accumulation and budget in the Bohai Sea, Yellow Sea and East China Sea. Mar. Geol. 390, 270–281.
Rahaman, W., Singh, S.K., Sinha, R., Tandon, S.K., 2009. Climate control on erosion distribution over the Himalaya during the past 100 ka. Geology 37, 559–562.
Rao, Z., Li, Y., Zhang, J., Jia, G., Chen, F., 2016. Investigating the long-term palaeoclimatic controls on the δD and δ18O of precipitation during the Holocene in the Indian and East Asian monsoonal regions. Earth Sci. Rev. 159, 292–305.
Rao, W., Mao, C., Wang, Y., Huang, H., Ji, J., 2017. Using Nd-Sr isotopes and rare earth elements to study sediment provenance of the modern radial sand ridges in the southwestern Yellow Sea. Appl. Geochem. 81, 23–35.
Reimer, P.J., Bard, E., Bayliss, A., Beck, J.W., Blackwell, P.G., Ramsey, C.B., Buck, C.E., Cheng, H., Edwards, R.L., Friedrich, M., Grootes, P.M., Guilderson, T.P., Haflidason, H., Hajdas, I., Hatté, C., Heaton, T.J., Hoffmann, D.L., Hogg, A.G., Hughen, K.A., Kaiser, K.F., Kromer, B., Manning, S.W., Niu, M., Reimer, R.W., Richards, D.A., Scott, E.M., Southon, J.R., Staff, R.A., Turney, C.S.M., Plicht, J.v.d., 2013. IntCal13 and Marine13 radiocarbon age calibration curves 0–50,000 years cal BP. Radiocarbon 55, 1869–1887.
Révillon, S., Jouet, G., Bayon, G., Rabineau, M., Dennielou, B., Hémond, C., Berné, S., 2011. The provenance of sediments in the Gulf of Lions, western Mediterranean Sea. Geochem. Geophys. Geosyst. 12, Q08006.
Romans, B.W., Castelltort, S., Covault, J.A., Fildani, A., Walsh, J.P., 2016. Environmental signal propagation in sedimentary systems across timescales. Earth Sci. Rev. 153, 7–29.
Saito, Y., Wei, H., Zhou, Y., Nishimura, A., Sato, Y., Yokota, S., 2000. Delta progradation and chenier formation in the Huanghe (Yellow River) delta, China. J. Asian Earth Sci. 18, 489–497.
Schouten, S., Hopmans, E.C., Sinninghe Damsté, J.S., 2013. The organic geochemistry of glycerol dialkyl glycerol tetraether lipids: a review. Org. Geochem. 54, 19–61.
Shao, J., Yang, S., 2012. Does chemical index of alteration (CIA) reflect silicate weathering and monsoonal climate in the Changjiang River basin? Chin. Sci. Bull. 57, 1178–1187.
Smith, D.E., Harrison, S., Firth, C.R., Jordan, J.T., 2011. The early Holocene sea level rise. Quat. Sci. Rev. 30, 1846–1860.
Song, B., Li, Z., Saito, Y., Okuno, J.i., Li, Z., Lu, A., Hua, D., Li, J., Li, Y., Nakashima, R., 2013. Initiation of the Changjiang (Yangtze) delta and its response to the mid-Holocene sea level change. Palaeogeogr. Palaeoclimatol. Palaeoecol. 388, 81–97.
Tütken, T., Eisenhauer, A., Wiegand, B., Hansen, B.T., 2002. Glacial-interglacial cycles in Sr and Nd isotopic composition of Arctic marine sediments triggered by the Svalbard/Barents Sea ice sheet. Mar. Geol. 182, 351–372.
Uehara, K., Saito, Y., 2003. Late Quaternary evolution of the Yellow/East China Sea tidal regime and its impacts on sediments dispersal and seafloor morphology. Sediment. Geol. 162, 25–38.
Wang, H., Yang, Z., Wang, Y., Saito, Y., Liu, J.P., 2008. Reconstruction of sediment flux from the Changjiang (Yangtze River) to the sea since the 1860s. J. Hydrol. 349, 318–332.
Wang, Y., Dong, H., Li, G., Zhang, W., Oguchi, T., Bao, M., Jiang, H., Bishop, M.E., 2010. Magnetic properties of muddy sediments on the northeastern continental shelves of China: implication for provenance and transportation. Mar. Geol. 274, 107–119.
Wang, Z., Zhan, Q., Long, H., Saito, Y., Gao, X., Wu, X., Li, L., Zhao, Y., 2013. Early to mid-Holocene rapid sea-level rise and coastal response on the southern Yangtze delta plain, China. J. Quat. Sci. 28, 659–672.
Wang, Y., Li, G., Zhang, W., Dong, P., 2014. Sedimentary environment and formation mechanism of the mud deposit in the central South Yellow Sea during the past 40 kyr. Mar. Geol. 347, 123–135.
Wang, Y., Wang, S., Liu, M., 2017. Magnetic properties indicate sediment provenance and distribution patterns in the Bohai and Yellow Seas, China. Cont. Shelf Res. 140, 84–95.
Wei, J., Shi, X., Li, G., Liang, R., 2003. Clay mineral distributions in the southern Yellow Sea and their significance. Chin. Sci. Bull. 48, 7–11.
West, A.J., Galy, A., Bickle, M., 2005. Tectonic and climatic controls on silicate weathering. Earth Planet. Sci. Lett. 235, 211–228.
Willenbring, J.K., von Blanckenburg, F., 2010. Long-term stability of global erosion rates and weathering during late-Cenozoic cooling. Nature 465, 211–214.
Woodward, J., Macklin, M., Fielding, L., Millar, I., Spencer, N., Welsby, D., Williams, M., 2015. Shifting sediment sources in the world's longest river: a strontium isotope record for the Holocene Nile. Quat. Sci. Rev. 130, 124–140.
Xiang, R., Yang, Z., Saito, Y., Fan, D., Chen, M., Guo, Z., Chen, Z., 2008. Paleoenvironmental changes during the last 8400 years in the southern Yellow Sea: benthic foraminiferal and stable isotopic evidence. Mar. Micropaleontol. 67, 104–119.
Xie, S., Evershed, R.P., Huang, X., Zhu, Z., Pancost, R.D., Meyers, P.A., Gong, L., Hu, C., Huang, J., Zhang, S., Gu, Y., Zhu, J., 2013. Concordant monsoon-driven postglacial hydrological changes in peat and stalagmite records and their impacts on prehistoric cultures in central China. Geology 41, 827–830.
Xu, K., Li, A., Liu, J.P., Milliman, J.D., Yang, Z., Liu, C.-S., Kao, S.-J., Wan, S., Xu, F., 2012. Provenance, structure, and formation of the mud wedge along inner continental shelf of the East China Sea: a synthesis of the Yangtze dispersal system. Mar. Geol. 291-294, 176–191.
Xue, C., Zhou, Y., Zhu, X., 2004. The Huanghe River course and delta from end of Late Pleistocene to the 7th century BC. Acta Oceanol. Sin. 26, 48–61.
Yang, S., Youn, J.-S., 2007. Geochemical compositions and provenance discrimination of the central south Yellow Sea sediments. Mar. Geol. 243, 229–241.
Yang, S.Y., Jung, H.S., Lim, D.I., Li, C.X., 2003. A review on the provenance discrimination of sediments in the Yellow Sea. Earth Sci. Rev. 63, 93–120.
Yang, S., Jiang, S., Ling, H., Xia, X., Sun, M., Wang, D., 2007a. Sr-Nd isotopic compositions of the Changjiang sediments: implications for tracing sediment sources. Sci. China Ser. D Earth Sci. 50, 1556–1565.
Yang, S., Wei, G., Xia, X., Sun, M., Tang, M., 2007b. Provenance study of the Late Cenozoic sediments in the Changjiang delta: REE and Nd isotopic constraints. J. Quat. Sci. 26, 339–346.
Yang, S., Wang, Z., Dou, Y., Shi, X., 2014. Chapter 21 A review of sedimentation since the Last Glacial Maximum on the continental shelf of eastern China. In: Geological Society, London, Memoirs. 41. pp. 293–303.
Zou, L., Hu, B.Q., Dou, Y.G., Li, J., Xie, L.H., Dong, Liang, 2017. Middle holocene organic carbon and biomarker records from the South Yellow Sea: relationship to the East Asian Monsoon. J. Ocean Univ. China (accepted).